CFD For Tail Rotor Design and Evaluation

Alan Brocklehurst[1], René Steijl and George Barakos

AgustaWestland and Department of Engineering, University of Liverpool,
Brownlow Hill, Liverpool L69 3GH, United Kingdom
e-mail: alan.brocklehurst@agustawestland.com or g.barakos@liverpool.ac.uk
[1]PhD Candidate and
Principal Engineer, Rotor Aerodynamics, Helicopter System Design, AgustaWestland (Yeovil).

Key words: Tail rotor design, tip shape, hover induced power, CFD.

ABSTRACT

In this paper, the Helicopter Multi-Block (HMB) CFD method has been used to evaluate the performance of a series of tail rotor tip designs. A good tip shape is essential for tail rotors since they need to generate a substantial amount of thrust from a limited blade area and tip-speed to provide both torque compensation and yaw manoeuvre capability without demanding excessive power. The design aim is to delay power divergence at the onset of stall at high pitch angles for tip Mach numbers in the region of 0.6, while seeking low noise and low vibration in forward flight. A means of accurately evaluating a new tip design is therefore an important element of the design process. The computational method was first validated against available published experimental data for both main and tail rotors, and is here compared to tests on a model tail rotor in hover, for blades having 0, 8 and 16 degrees of twist. All the rotor designs considered here are developed from the datum rectangular model tail rotor blade, and employ a NACA0012 aerofoil with zero twist. A series of tail rotor blades were designed with different tip shapes, including a square-cut tip, a volume-of-revolution tip, a swept-leading-edge, a parabolic tip, and several Kuchemann-type tips. In addition, some of the designs incorporated anhedral. Following Euler evaluation in hover, three designs were compared in forward flight, and further results have been obtained for these selected blades using Navier-Stokes in hover. Overall, the results of the computations indicate that, at low thrust, the Euler equations are adequate to represent the impact of the design changes, at least as far as the induced power is concerned, while use of Navier-Stokes provides a more complete assessment of tail rotor characteristics as the pitch setting and thrust becomes higher. The effects of twist and anhedral were well-represented, and in hover it was found that anhedral off-loads the tip, increasing the loading at mid-radius, in a broadly similar manner to twist. The Navier-Stokes method provides an indication of the stall development which is so important for tail rotor design, and the availability of an unsteady RANS method with sliding planes can extend the evaluation to include fin blockage. It is concluded that the Helicopter Multi-Block (HMB) CFD method has the resolution to highlight differences in tip shape and is well suited for the design and analysis of helicopter blades.

INTRODUCTION

The need to achieve better performance from all types of helicopter rotors leads to the need to predict the impact of new blade designs with greater precision than ever before. This paper reports recent progress in the application of the Helicopter Multi-Block (HMB) CFD code to rotor design, focusing on tail rotors in particular.

The demands placed on helicopter tail rotors are such that the maximum possible thrust must be delivered from the available blade area and tip-speed.

Tail rotors operate at high pitch and high disc-loading in-and-around hover. The tip must therefore perform well at high-lift and mid Mach numbers, but must also alleviate compressibility problems in forward flight. This is especially true in the region of the blade tip, where the flow is highly 3-dimensional and both these effects are important.

The application of the CFD method lends itself to the solution of this problem, starting with the surface geometry for the generation of the grid, together with the flow conditions, it avoids any assumptions of wake structure which is often implicit in lower-order design methods. Instead, the CFD approach makes use of the fundamental laws of conservation

Presented at the 34th European Rotorcraft Forum, Liverpool, UK, September 16-18, 2008.

for mass, momentum and energy to obtain a truly 3D solution for the entire compressible and viscous flow field around the rotor. This approach is therefore ideally suited to the evaluation of blade tip designs.

In this paper, a comparison of several tail rotor designs is presented in an effort to develop understanding of the influence of tip shape on rotor performance and to quantify the effects of the various design features such as blended Kuchemann tip shapes, anhedral and twist. All results presented in this paper have been obtained using the Helicopter Multi-Block solver (HMB) [Ref. 1 and 2].

The paper begins with a brief presentation of the solver and describes its validation using available experimental data. Results from the HMB method are then further compared to existing model rotor data. The model rotor tests include thrust-power-pitch measurements for a range of tip Mach numbers for blades with 0, 8 and 16 degrees of linear twist, together with flow visualisation of the rotor wake which yields vortex positions in the wake for the zero-twist datum blades at 4 different pitch angles. This step is followed by presentation of the various tail rotor blade tip designs considered during this study along with the results obtained for each design at a range of pitch angles for isolated rotors in hover. The effects of tip shape and anhedral are then considered in forward flight to confirm that no severe restriction on control loads arise from the total blade pitching moments. Comparisons are then made with the results of viscous hover simulations for a selection of tip shapes, and results are also shown at high pitch angle as the stall is approached. A summary of the findings along with suggestions for further work are given at the end of the paper.

HELICOPTER MULTI-BLOCK SOLVER

The Helicopter Multi-Block (HMB) solver has been under development at the University of Liverpool for the past three years and has been validated and demonstrated for a range of test cases related to helicopter flow analysis and design.

The unsteady Navier-Stokes equations are discretised on a curvilinear multi-block body conforming mesh using a cell-centred finite volume method. The convective terms are discretised using Osher's upwind scheme [Ref. 3]. MUSCL variable extrapolation is used to provide second-order accuracy with the Van Albada limiter. A central discretisation method is used for the viscous terms. The solver includes a range of one- and two-equation turbulence models and a Smagorinsky LES and Spalart-Almaras DES model. The turbulence model used in the hover Navier-Stokes applications reported in this paper was a variant of the k-ω model. A dual-time stepping method is employed for time-accurate simulations, where the time derivative is approximated by a second-order backward difference [Ref. 4]. The resulting non-linear system of equations is solved by integration in pseudo-time using a first-order backward difference. In each pseudo-time step, a linearisation is used to obtain a system of equations, which is solved using a Generalised Conjugate Gradient method with a Block Incomplete Lower-Upper (BILU) pre-conditioner.

The HMB solver makes use of a special scheme for the actuation of rotor blades [Ref. 2]. The “hover formulation” allows the computation of hovering rotor flows as steady-state cases resulting in higher throughput where several rotors have to be tested at a range of thrust settings. In addition, a rotor trimmer is also implemented in HMB and can be used for the analysis of rotors at a specific thrust, either in hover or forward-flight.

To obtain an efficient parallel method based on domain decomposition, the method should have a good serial performance when applied to the domains allocated to the different processors, combined with minimal communication. To achieve this aim, the flow solver uses the following method.

The flux Jacobians resulting from the linearisation in pseudo-time are employed in an approximate form that reduces the number of non-zero entries and as a result the size of the linear system is also reduced. The use of the approximate Jacobian also reduces the parallel communication since only one row of halo cells is needed by the neighbouring process in the linear solver instead of two in the case of an 'exact' Jacobian.

a) The communication between processes is minimised by decoupling the BILU factorization between blocks.
b) On each processor a vector is allocated that contains all the halo cells for all grid

blocks.

c) Inter-process communication is performed by sending a series of messages between the respective processes, each corresponding to a block connection, containing the halo cell data. The messages are sent in chunks of 10,000 double precision numbers using non-blocking send and receive MPI functions.

This method has been used on a range of platforms, including multi-processor workstations and Beowulf clusters consisting of various generations of Pentium and Opteron processors. The solver has been ported to the HPCx computer at the Daresbury Laboratory.

GRID GENERATION

Accurate representation of the blade geometry is paramount and this can be achieved with modern CAD tools, such as Rhino, or CATIA, and a genuinely multi-block grid approach. The current technique is based on the idea of surrounding the blades in "rigid" blocks of high-quality grids and accounting for changes of pitch and rotation by deforming the surrounding domain. The grids developed for this work were generated using ICEM-CFD Hexa and then converted into a format suitable for the HMB solver. A typical calculation involves about 250 blocks per blade and is computed on 16-128 processors according to the grid density and solver options employed.

The current topologies combine an H-type structure away from the blades with a C-type structure attached to them. This allows for accurate computation of viscous cases and provides a mechanism for pitching the blades with the near-blade-grid remaining in an un-deformed state. Where grid deformation is needed this is done via trans-finite interpolation (TFI). Figure 1 shows the periodic domain of the blade and provides details of the two main types of surface topology for rectangular and Kuchemann tips. For the hover cases a cylindrical hub was used for convenience, for both Euler and Navier-Stokes simulations. Grid dependency checks were carried out by both decreasing and increasing the number of grid points, and the current grid size of about 2.5 million points for Euler was shown to be adequate [Ref. 12]. For the Navier-Stokes simulations grid sizes up to about 8 million points per blade were used.

VALIDATION

Validation results for hovering rotors, and rotorcraft flows in general, computed with HMB have been previously presented [Ref. 1-2,5-6]. In fact, a validation database has been compiled at the University of Liverpool CFD Lab comprising validation cases for aerofoils, wings, unsteady stall, and hovering and forward flying rotors. This database is gradually expanding as new cases become available.

COMPARISON OF CFD WITH MODEL TAIL ROTOR DATA IN HOVER

Further comparisons with model rotor test data are presented. This set of results corresponds to model rotor tests conducted by the first author at Westland Helicopters in 1980-84. For the (datum) rectangular blade design, thrust, power, pitch and vortex wake measurements are available from tests on a 4-bladed model rotor with 0, 8 and 16 degrees of twist. This data was used to confirm the trends of the Euler CFD predictions in hover before going on to explore the new tip shapes. Excellent agreement was obtained which established confidence in the CFD method and the grids.

The model rotor had stiff composite blades of NACA0012 aerofoil section, with the first aerofoil located at 1/3 radius. The radius of the blade was 21" (533.4mm) by 3.28" (83.3mm) chord, giving R/c=6.402. In the tests, the tip Mach number ranged from 0.263 for the flow visualisation up to a maximum of 0.492 for the force measurements. The model rotor hover tests were carried out in a large rectangular building measuring 30ft by 45ft by 20-25ft high, and were free from recirculation as confirmed by wool-tuft wand visualisation.

Thrust-pitch and power comparisons are shown in Figure 2. The CFD solver produced results which are in good agreement with the test for the thrust-pitch characteristics, Figure 2(a), while for comparison a lifting line and prescribed wake method tends to over-predict the lift-curve. This set of results was also plotted in the form of C_Q vs $C_T^{3/2}$ (Fig. 2b) and a polynomial of second order was fitted to the thrust data to reveal a reduction in induced power factor with increased twist. Of course, this set of results lacks the viscous contributions to power and consequently falls well below the experimental data which relate

to the model tail rotor at relatively low Reynolds number. On the other hand, the predictions show the correct trends for induced power, and results are as expected for inviscid flow simulations. The CFD results for the 0, 8 and 16 degree twisted blades correspond to induced power factors of 1.40, 1.34, and 1.20 respectively.

The spanwise loading distribution is shown in Figure 3, and the effect of twist is clearly demonstrated. The results show the expected increase in inboard loading with a corresponding reduction in the tip region. On the same Figure, results from a prescribed wake hover prediction method are also plotted. Not surprisingly, most of the differences between the two methods are concentrated in the non-linear tip region. The results from the CFD include a loading spike near the extreme tip due to the suction on the blade underneath the tip vortex. Whilst a Navier-Stokes solution would provide a better model for certain tip geometries, these preliminary Euler results do capture this important effect.

Looking at the pitching moment, a reduction in the moment coefficient due to increased twist is shown in Figure 3(b). The effect of the suction on the extreme tip edge is clear, and just inboard of the tip this is counter balanced by a nose up moment arising from the clustering of isobars in the forward leading edge corner of the rectangular blades.

The model tail rotor tests also included visualisation of the wake for the zero-twist blades using directed stroboscopic lighting and a simple phase delay so that the vortex locations could be measured at increasing wake ages. Measurements were taken on-screen using a calibrated video position analyser and each point represents a time-averaged result.

Figure 4 compares predicted and measured vortex displacements for the base-line configuration showing excellent agreement between HMB predictions and measurements. Also included are the prescribed wake predictions of Kocurek and Tangler, [Ref. 9], and the CFD lies between these bands, very close to the test data. The CFD also reveals some small non-linear variations in the vortex displacements, and more particularly, lobes (between blade passages) in the wake contraction which appear to be reflected in the experimental results. The wake visualisation tests were conducted in a large hover test facility as noted above, with reduced tipspeed to avoid any danger of re-circulation, and the blades were accurately balanced and tracked to a high standard to avoid vortex gearing.

TAIL ROTOR BLADE DESIGNS

Figure 5 illustrates the various tip shapes which were created by modification of the rectangular baseline rotor blade. The blade surfaces were generated using Rhino solid modelling software. The baseline blade was chosen to be consistent with the zero-twist model rotor blade that was used in the hover tests. The aim was to identify a favourable tip shape for tail rotor applications through use of CFD analysis. The tip shape must be suitable for high-lift conditions at mid, sub-sonic tip Mach numbers, in the region of 0.6, and should both alleviate the bunching of the isobars at the forward tip corner as well as suppressing stall and encouraging an efficient vortex roll-up. In operations near hover and below stall, a reduction in induced power, or an improvement in Figure of Merit is highly desirable. In forward flight, the trends towards low aspect ratio tail rotor blades provides some tip relief such that sweep is not essential, and the designs considered here employs a constant aerofoil section. Recent tail rotor design work at AgustaWestland has employed high-lift aerofoils and a reduction of camber and thickness in the tip region, together with a moderate amount of twist. However, the blade designs considered here all employ a NACA 0012 aerofoil and zero-twist, with the aim of comparing the tip design. The Kuchemann-type tips were included as they are expected to have good performance at high pitch in hover, as well as in forward flight. The opportunity was also taken to explore the use of anhedral because it had previously shown potential for low induced power on main rotor designs and propellers.

INVISCID TAIL ROTOR CFD IN HOVER

In keeping with the model rotor tests, the CFD simulations reveal results for the overall performance of the rotor and the induced and profile power contributions are naturally combined. The CFD results were therefore analysed using techniques developed for parameterising model rotor data during later

tests involving Rectangular and Vane Tip model main rotor blades [Ref 10]. For the Euler solutions from HMB, the power losses are small, and the main interest in this part of the work was to identify differences in induced power. The induced power factor, k_i, was determined by plotting C_Q versus $C_T^{1.5}$ and using a second order curve fit to consistently determine a value of the slope, the 'experimental points' in this instance being provided by the CFD, which was well converged in all cases. As in the model rotor tests, it is important to have enough points at sufficiently low pitch to provide a good fit. The coefficient of the second order term in all cases was found to be relatively small, suggesting that k_i is independent of C_T for the tip designs and blade loading considered here, despite the potential for non-linear vortex wake effects. While it is always difficult to truly separate induced and profile power, for the Euler results the 'profile power' only arises from numerical effects, and is at most only about 1/10 of the normal value, below the point where the Euler solution breaks down at higher incidences. The results were confirmed by plotting the residual 'profile power' against blade loading to ensure that it followed a realistic trend once the induced power had been subtracted according to the curve fit. This approach was used to compare all the different tip designs at low to moderate thrust level, as illustrated in Figure 6(a) and (b).

The CFD results for various tip designs are compared for untwisted blades with the same NACA0012 aerofoil, at a typical full-scale Mach number of 0.6. All CFD grids have been refined to allow a similar resolution of the wake for which vortices can be seen for one complete revolution (4 blade passes). Figure 7 shows a comparison of Euler results in terms of rotor torque, Figure 7(a), and FoM, Figure 7(b), and induced power factor, k_i, Figure 7(c), for several tail rotor designs in hover, and reveals benefits due to tip shape and anhedral.

The induced power factor for the datum blade was found to agree well with experiment (Figures 2b and 6a), and gives confidence in the method. Note that the k_i for a tail rotor is normally significantly greater than that for a main rotor and the correct trends have also been seen in similar computational studies for main rotors.

Euler results for Figure of Merit in Figure 7(b) are, of course, higher than they would be in reality due a lack of viscosity. To overcome this for initial design comparisons, ahead of the Navier-Stokes results, an arbitrary constant skin friction or profile drag coefficient was added to the raw computational results. For a tail rotor a value of CD_{sf}=0.008 seems most appropriate, and this value was arbitrarily added regardless of tip shape. Taking this into account naturally reduces the sensitivity of the results for the very low pitch cases, and provides realistic FoM values at more moderate thrust coefficients, as shown by the lines with open symbols in Figure 7(b).

In particular, the results show clear benefits of using a well designed tip shape and anhedral, and suggest that these benefits are cumulative. The set of results obtained from the CFD analysis allows insight to be developed for the performance of each tip shape. Clearly, the datum blade has the highest induced power (for the results illustrated here) though differences between the designs are subtle and CFD is perhaps the only method capable of demonstrating and separating these. The quarter-chord wide Kuchemann-type tip shape of TRB-001 is clearly superior to the datum rectangular blade, TRB-000, while TRB-005 appears to perform very well in comparison with the TRB-001 design. The rectangular anhedral tip, TRB-004, is similarly better than the datum blade. The 1/2c wide Kuchemann tip showed no improvement relative to the datum blade, possibly due to a less clean roll-up. The Swept L.E. tip showed a small improvement, but also exhibited higher residual 'profile power' losses. The volume-of-revolution tip, TRB-006, also shows a substantial improvement, due to the cleaner flow over the tip edge. The parabolic tip, TRB-007, has a good Figure of Merit, but revealed a lower thrust-pitch gradient than the other blades.

The observed changes in the performance due to the various tip configurations can be explained by comparing the vortex wake trajectories, as shown by the example in Figure 8, and the blade-loading distributions, Figure 9. For the blades with anhedral, TRB-004 and TRB-005, the vortices are predicted to pass closer to the following blade (the first author has noted such behaviour in tests on other types of blades, not presented here), and their subsequent displacement is slightly reduced,

as in Figure 8.

The comparison of the loading and moment distribution of the TRB-005, Kuchemann tip with anhedral, and TRB-001, the same tip but without anhedral, is significant. As can be seen in Figure 9, the anhedral reduces the tip loading and slightly increases the loading inboard. This result is reminiscent of the results found earlier for the twisted model rotor blades, and it may be deduced that anhedral acts in a broadly similar manner as twist, except that the effect is not present near the root of the blade.

Clearly, CFD is a reliable tool for the analysis of the rotor performance, and is particularly useful when advanced tip configurations are being explored. The comparison between the effects of anhedral and twist generate quite useful insights in terms of the design of tail rotors, suggesting that a design engineer can select between twist and anhedral as a mechanism for reducing tip loading or even opt for a combination of the two contributions. This is a good example of how CFD can be used to generate useful understanding for design purposes.

FORWARD FLIGHT ASSESSMENT OF SELECTED TIP DESIGNS

Three of the tip shapes considered were selected for evaluation in forward flight, namely the datum blade, TRB-000, the flat, 1/4c wide Kuchemann tip, TRB-001, and the 20 deg anhedral 1/4c wide Kuchemann, TRB-005. A typical helicopter high-speed cruise case of 160kts was chosen for these comparisons, giving an advance ratio of about 0.4 based on the same full-scale tip Mach number of 0.6, as used in the hover comparisons. In order to determine the thrust and flapping, the model rotor dimensions were scaled up by 2.25 times, to produce a tail rotor suitable for a typical Lynx-size helicopter. Using typical values for Lock number, and assuming that about 50% of the typical tail rotor thrust requirement would be supplied by fin off-loading, a simple momentum-based tail-rotor program was used to determine the collective pitch and flapping, taking into account conventional pitch-flap coupling. The nominal thrust coefficient was C_T(UK)=0.019, or C_T(US)=0.0096. Further calculations were also undertaken using an in-house forward flight program to confirm the collective pitch, determine the blade loading and vortex intersection pattern, and to obtain a first estimation of blade pitching moments due to pitch-rate effects for the datum rectangular blade. The following trim conditions were used as input for the HMB CFD code:

Advance Ratio = 0.4032,
M_{fwd}=.24193, M_{tip}=0.6,
Collective Pitch = 4.0 deg (no twist),
e_{flap}=0.065R, 45 deg pitch-flap coupling.
Coning: β_0=0.6689 deg.
Flapping (degrees, negative Fourier series):
β_{1c}=1.7971, β_{1s}=-1.3773
β_{2c}=0.1016, β_{2s}=0.0347

All the tail rotor blades were run at the same pitch angles for expediency. In retrospect, it may be more desirable to adjust the trim to provide a comparison at the same thrust, since the CFD showed that the style of the tip has an influence on the thrust (and a small effect on flapping). This is perhaps more significant for a main rotor, than for the current evaluation which assumes significant tail rotor off-loading from the fin.

Despite the low R/c which provides some tip relief, a fairly strong shock occurs on the NACA0012 blades in this high speed case. Figure 10 compares the selected blades at the four cardinal azimuths. The results on the advancing side of the disc show how the isobars curve-back in the extreme tip region to provide further relief for the Kuchemann tip, TRB-001, relative to the datum blade TRB-000. Similar patterns, with perhaps more relief, are seen for the anhedral blade, TRB-005, and difference in the isobar patterns are observed at the front and rear of the disc. The CFD results reveal how the tip loading is influenced in detail by the tip shape, as the blades undergo the effect of changes in incidence, side-slip, and varying Mach number around the azimuth.

The vorticity in the wake for the forward flight case is illustrated in Figure 11. Note that, at the advance ratio of 0.4, the retreating blade is about to encounter the trailed vortex from the preceding blade which is at the rear of the disc. This interaction produces transient airloads which give a nose-down pitching moment at about 280 degrees for each of the blade designs. While the Euler solution may have broken down prematurely during this

interaction, such transients will occur in practice, depending upon the advance ratio, thrust and flapping.

The aerodynamic pitching moments obtained from the CFD simulations are compared in Figure 12. Here the datum blade is first compared to a lifting-line forward flight program prediction, Figure 12(a), and it can be seen that while the peak-to-peak variation is similar, the inviscid computational results are offset due to compressibility effects and the fact that the aerofoil data for NACA0012, as used in the performance program, contains a small positive moment coefficient, depending upon the incidence and Mach number.

The total blade pitching moments for the three tip shapes are compared in Figure 12(b). There is little difference in the results for the datum and (flat) Kuchemann tip, while the anhedral blade, TRB-005, shows a slightly larger peak-to-peak variation, and an increased nose-up moment in the first quadrant, indicating a phase-shift.

In order to gain further insight, the computational results were the subject of a Fourier analysis which identified the phase shift in the first harmonic as almost 50 degrees for TRB-005 relative to TRB-001, due to anhedral. The mean, first and second harmonics were reconstructed, as in Figure 12(c). For illustration and comparison, this figure also contains a moment variation arising from use of a typical cambered tail rotor aerofoil with an arbitrary (constant) pitching moment coefficient of -.02. It is clear that this variation is approximately in anti-phase to the predicted moments from the computational results for the anhedral tip, and the combined effect is illustrated by the dashed line which contains mainly second harmonics.

Of course, the aerodynamic loading only makes up part of the total tail rotor control loads, and may, in fact, only account for about 25% of the pitching loads for wide-chord tail rotor blades which operate at relatively high rotational speed. Nevertheless, the current work illustrates the usefulness of CFD for determining rotor aerodynamic moments (which may take on even greater importance in main rotor applications) and has confirmed that tip anhedral may be a viable solution for tail rotor applications. Improved accuracy would be obtained by using Navier-Stokes solutions for further evaluations of a final design, where separation may occur if more highly loaded cases were considered.

VISCOUS TAIL ROTOR CFD IN HOVER - RESULTS AND COMPARISONS

In this part of the work, the Navier-Stokes method has been used to extend the simulations to include viscous effects which are dominant at high pitch angles near stall. The initial Euler studies, described above, were primarily intended for selecting which of the various design would be the subject of a computationally more expensive Navier-Stokes flow simulation.

The quantification of viscous effects was the first objective set for this phase of the work which started with the TRB-005 design, due to its good performance characteristics in terms of induced power factor (Figure 7(c)).

For consistency, all the vortex trajectories shown in this paper were extracted from Tecplot's vorticity contours for both the Euler and Navier-Stokes solutions using sections in a vertical plane. However, an improved technique has also been developed using the λ_2 parameter, as described by Jeong and Hussain [Ref.11], to better resolve the precise location of wake vortices.

Figure 13 presents a comparison between viscous and inviscid solutions for the vertical displacement of the tip vortex for the anhedral blade, TRB-005. The viscous results (using up to about 8 million points) have the same trend as the inviscid ones (2.8 million points) and the two sets of data agree well very close to the tip. Further away, the Navier-Stokes solution indicates a slightly larger wake radius, as might be expected due to viscous losses, Figure 13(a). In the viscous case, the vertical displacement is generally increased by a small amount as shown in Figure 13(b).

Vertical displacement and wake contraction positions extracted from HMB viscous results for the Kuchemann-type tips, TRB-001 and 005 (the latter with anhedral), are shown in Figure 14. The vertical displacement graph again shows that the vortex from the anhedral tip remains fairly level, relative to that from the tip without anhedral, and passes slightly closer

below the following blade, Figure 14(a). However, for the viscous results obtained to date, the difference is now less marked than it was for Euler. Shortly after the impetus from the following blade, the two displacement curves come together. Further down the wake, the vortices from the anhedral blade show a lower displacement, as noted previously for the Euler solutions (Figure 8). While the initial contraction is apparently not affected by anhedral, a small difference appears between 90 and 180 degrees of wake-age, Figure 14(b), and the anhedral blade produces a slightly greater final contraction. As before, the contraction-rate varies between blades passes.

Both sets of viscous results, for TRB-001 and TRB-005, show a reduced contraction in the far wake compared to the Euler results presented in the first part of this paper.

Overall, the viscous results obtained to date confirm the benefits of anhedral at a moderate pitch angle of 10 degrees. However, further viscous cases are required to fully define the induced power factor and overall thrust-power characteristics.

NAVIER-STOKES COMPUTATIONS AT HIGH PITCH ANGLES IN HOVER

Perhaps the most important aspect of tail rotor design is to achieve a maximum thrust capability (in or near hover) within design constraints of, say, blade area and tip-speed, whilst achieving acceptable forward flight characteristics. Indeed, the tail rotor must provide both torque compensation and manoeuvre thrust at all flight conditions, including the extremes, such as hot and high, and at ever increasing gross weights. The tail rotor therefore may frequently encounter conditions approaching stall, and this places emphasis on a tip shape which not only gives low induced power, but perhaps more importantly, is designed to delay stall onset, and minimise the rate of increase of power as the stall is reached.

During the design process, it is therefore essential to be able to accurately evaluate the characteristics of tail rotors at high pitch angles in order to be able to select the most suitable blade for the task, within given constraints. Previously, most CFD simulations have avoided any significant amount of separated flow, and indeed, as more of the blade enters stall an unsteady solution would be required, and this is the next logical step.

The work presented here, continues from the point where an Euler solution breaks down, and explores the use of a steady Navier-Stokes solution at higher incidences up to the point where the stall is reached for the datum rectangular, untwisted tail rotor blade. The aim this research is to use this approach to compare the performance of selected tail rotor tip designs, such as TRB-001 (Kuchemann Tip) and TRB-005 (Kuchemann tip with Anhedral), at high pitch angles.

As before, the grids were prepared in ICEM Hexa, having previously drawn a series of frames around the blade in Rhino, to provide curves to help control the positioning of grid blocks adjacent to the blade. The multi-block grid comprises 6,740,128 points in 205 blocks for the datum blade. Variation of pitch angle may be achieved by either rotating the geometry and re-projecting the grid, or by manipulating the grid using a 'Grid-Trimmer' program, Steijl [Ref. 2]. This later method provides a rapid means of changing pitch angle, while maintaining the mesh quality in blade-fixed blocks.

Figure 15(a) shows the Navier-Stokes results for the datum blade compared to the earlier Euler predictions for thrust-pitch, while the thrust-power characteristics are shown in Figure 15(b). The increased profile power due to viscous pressure losses and skin-friction are immediately clear. If the previously determined (Euler) induced power factor is assumed (in the absence of further results at low pitch), the profile drag can be deduced, Figure 15 (c), and the values also reflect the low Reynolds number of 1.168 million for Mtip=0.6 for the model rotor. As expected, the profile power diverges as the tip of the blade encounters stall. The blade aerodynamic pitching moments can also be seen to diverge, as expected, in Figure 15(d).

The pressure contours shown in Figure 16 confirm that the flow is attached at 15 degrees and below, while at 18 and 20 degrees the flow

increasingly separates near the tip of the blade.

The extent of the stalled flow is evident in the radial blade loading distribution, as shown in Figure 17. Near the tip, the loading peak is seen to collapse as a consequence of the separated flow, leading to a rounding off of the thrust-pitch curve and power divergence.

Exploration of tail rotor performance beyond pitch angles, of say, 16-18 degrees, calls for the use an unsteady RANS approach, and work is in progress towards this goal.

UNSTEADY NAVIER-STOKES FOR THE FIN-BLOCKAGE PROBLEM

Once an unsteady formulation has been adopted there is an opportunity to include another practical feature which has significant influence on tail rotor performance, namely fin-blockage. Sliding planes, [Ref. 1 and 2] were researched for use with HMB, primarily to model the main-rotor / fuselage interaction, and this technique also lends itself to the solution of the tail rotor fin blockage problem. A CFD simulation has therefore been constructed to compare with existing model rotor fin-blockage tests, which included wake flow visualisation, fin-pressure measurements, and smoke/tuft visualisation of the flow over the fin. A relatively low pitch angle of 8 degrees has been chosen to compare with the available data before progressing to more extreme pitch conditions. Figure 18 shows the experimental set up, and Figure 19 illustrates the equivalent tail rotor and fin geometry from which the mesh was generated. As measured in the tests, the rotor blades have a coning angle of 0.4 degrees and a small, first harmonic cosine flapping motion, of 0.1 deg, arising from the non-periodic nature of the flow. This prescribed blade motion has therefore been included in the simulations which are currently under-way.

The use of an unsteady Navier-Stokes formulation also allows the inclusion of additional features such as the feathering bearings, and this will further improve the realism of the simulation, since the wake from the pitch-bearings will have an effect on the root vortex. The fin (for this pusher tail rotor configuration) provides a ceiling effect which reduces the descent rate of the tip vortices and causes the wake to contract more as the blade passes over the fin.

SUMMARY AND FUTURE STEPS

A rotor CFD tool has been used to evaluate the performance of a set of generic tail rotor blade designs. The method has been well validated against published experimental data and further comparisons against the model rotor tests have been presented here.

Thrust-pitch characteristics and induced power factors deduced from the Euler computations were found to agree well with experiment, for a range of twisted tail rotor blades, and the vortex locations in the wake are generally well predicted.

The results of the CFD simulations have revealed subtle differences in the performance of the various tip shapes, and the HMB method has been found to be robust and reliable across a wide range of blade designs and conditions. The effect of anhedral has been shown to have a beneficial impact on the performance in hover, resulting in a better distribution of span-wise loading. Unsteady CFD forward flight simulations revealed a modest rise in the aerodynamic pitching moments, and has provided a valuable insight into tip aerodynamics of tail rotors.

Euler computations were used in the initial stages of this research due to their efficiency, and this strategy has allowed a wide range of designs to be considered and evaluated. Later comparisons against Navier-Stokes solutions show that less ultimate contraction is achieved when viscous effects are present.

A steady Navier-Stokes simulation has been successfully used to provide a prediction of the power divergence of a tail rotor at high pitch angles approaching stall. As the stall develops at higher angles, an unsteady solution becomes desirable to handle the unsteady vortex shedding.

Adoption of an unsteady CFD approach allow other practical features, such as feathering bearings and bluff root-end geometry to be represented, and the use of sliding planes enables the simulations to be extended to include fin blockage. The unsteady RANS

approach may also be used to simulate pitch transients.

At high pitch, the emphasis moves away from induced power factor and Figure of Merit to the need to suppress the power divergence experienced at the onset of stall. The nature of this divergence will depend on the selected tip shape, aerofoils and twist. The fidelity of the HMB method facilitates an evaluation of these effects.

ACKNOWLEDGEMENT

The authors wish to thank Robert Harrison, AgustaWestland (Yeovil), and Richard Markiewicz of DSTL, for permission to publish the model rotor data.

REFERENCES

[1] G. Barakos, R.Steijl, K. Badcock and A. Brocklehurst, *"Development of CFD Capability for Full Helicopter Engineering Analysis"*, Proceedings of the 31st European Rotorcraft Forum, 13-15 September 2005, Florence, Italy.

[2] R. Steijl, G. Barakos and K. Badcock, *"A Framework for CFD Analysis of Rotors in Hover and Forward Flight"*, Int. J. for Num. Meth. in Fluids, Vol. 51, 2006, pp. 819-847.

[3] S. Osher and S. Chakravarthy, *"Upwind Schemes and Boundary Conditions with Applications to Euler Equations in General Geometries"*, Journal of Computational Physics, Vol 50, 1983, pp. 447-481.

[4] A. Jameson, *"Time Dependent Calculations using Multigrid, with Applications to Unsteady Flows past Airfoils and Wings"*, AIAA Paper 91-1596, 1991.

[5] A. Spentzos, G. Barakos, and Badcock, P. Richards, B.E. Wenert, S. Schreck, and M. Raffel, *"CFD Investigation of 2D and 3D Dynamic Stall",* AIAA Journal, Vol 34, No 5, 2005, pp. 1023–1033.

[6] R. Morvant, K. Badcock, G. Barakos, and B.E. Richards, *"Aerofoil-Vortex Interaction Using the Compressible Vorticity Confinement Method",* AIAA Journal, Vol 43, No 1, 2004. pp. 63–75.

[7] M. Dindar, et al.,"*Effect of Tip Vortex Resolution on the UH-60A Rotor Blade Hover Performance Calculations*", 54th Annual Forum of the American Helicopter Society, Washington, D.C., May, 1998.

[8] P.F., Lorber, "*Aerodynamic Results of a Pressure-Instrumented Model Rotor Test at the DNW*", Journal of the American Helicopter Society, Vol 36, No 4, 1991.

[9] J.D. Kocurek and J.L. Tangler, *"A Prescribed Wake Lifting Surface Hover Performance Analysis"*, Proceedings of the 32nd Annual Forum of the American Helicopter Society. Washington, D.C. May 10-12, 1976.

[10] A. Brocklehurst, and A. Pike, "*Reduction of BVI Noise Using a Vane Tip*", AHS Specialist's Conference, San Francisco, January, 1994.

[11] J. Jeong and F. Hussain, *"On the identification of a vortex"*, J. Fluid Mechanics, Vol. 285, 1995, pp. 69-94.

[12] A. Brocklehurst, R.Steijl, and G. Barakos, "*Using CFD to Understand and Evaluate Tail Rotor Blade Designs",* AHS Aeromechanics Specialist's Conference, San Francisco, CA., Jan. 23-25, 2008

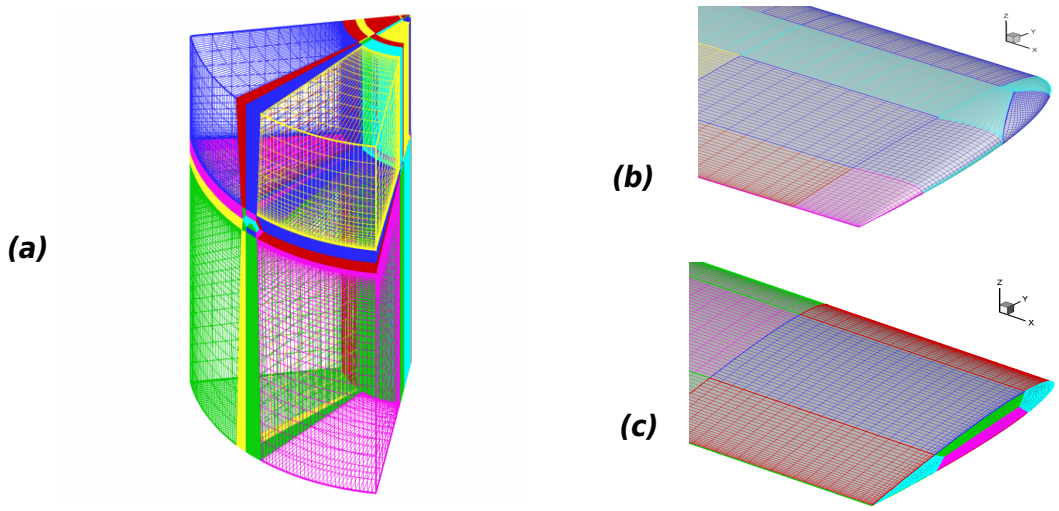

***Figure 1**. (a) Multi-block grids are employed with HMB for the analysis of tail rotor designs. The surface topology in (b) is compatible with TRB-001, 002, 003 and 005, and the simpler topology in (c) was used for TRB-000, 004, 006 and 007.*

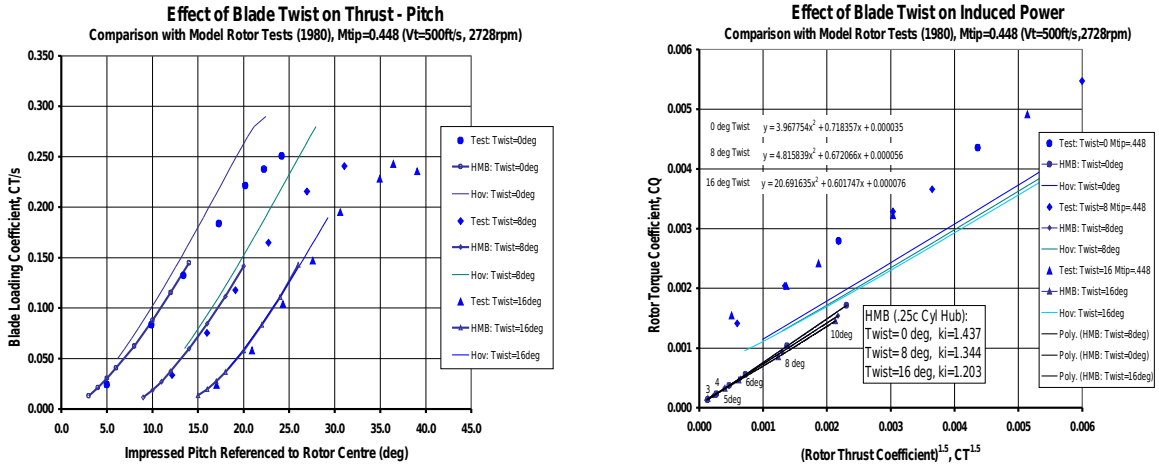

***Figure 2.** Comparison of CFD results with Model Tail Rotor Test Data. (a) thrust-pitch for 0, 8 and 16 degrees twist, b) also shown are results from prescribed wake hover program for comparison.*

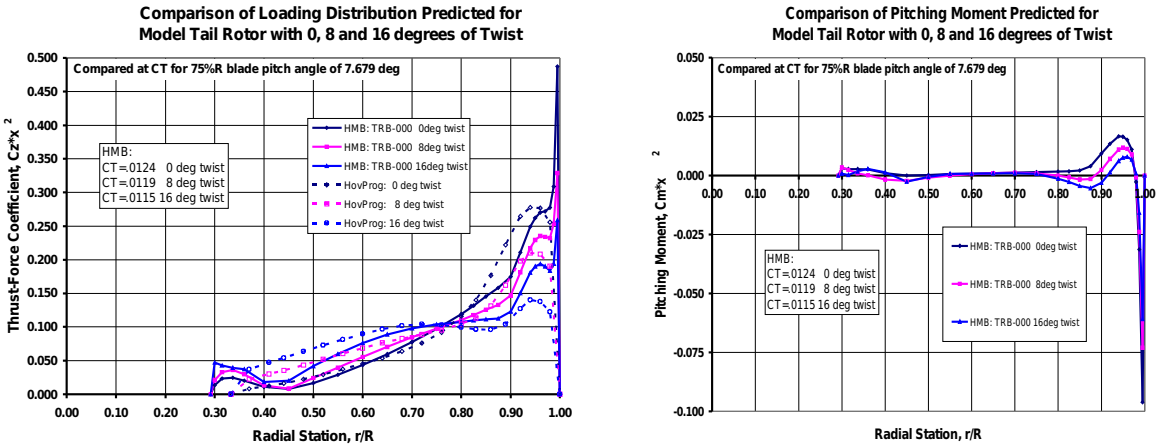

***Figure 3.** Assessment of the effect of twist. (a) span-wise loading and (b) span-wise moment distributions.*

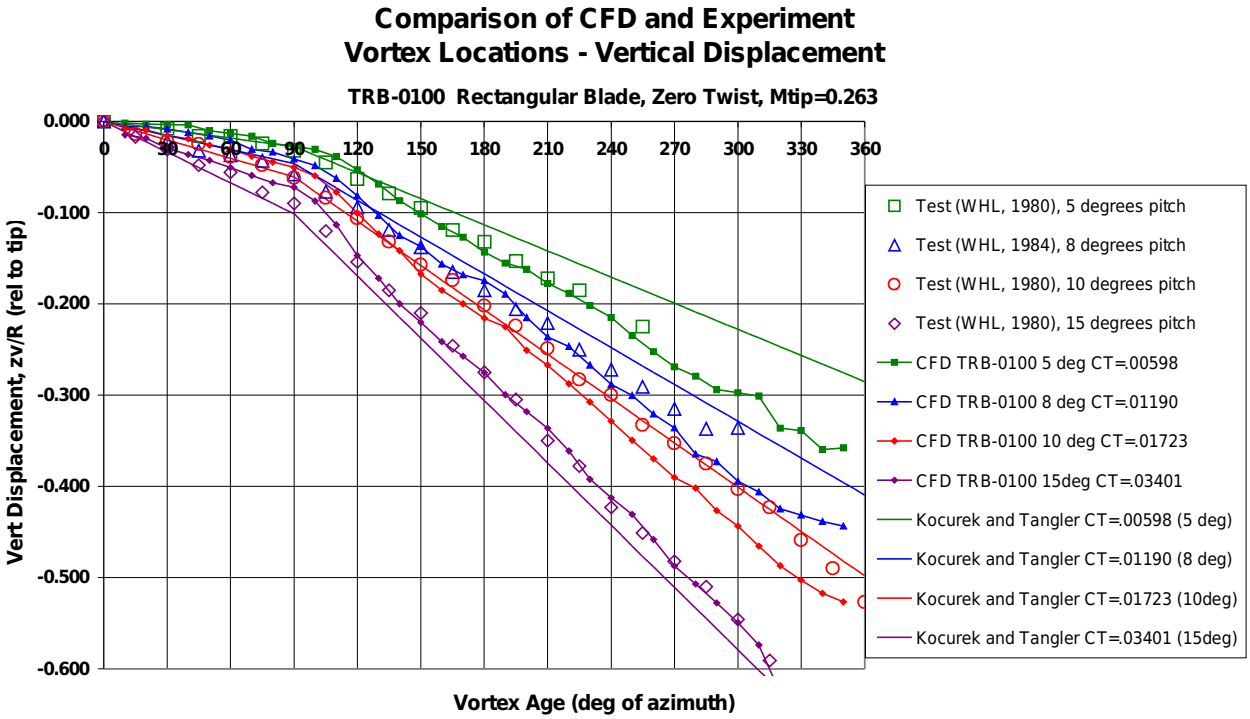

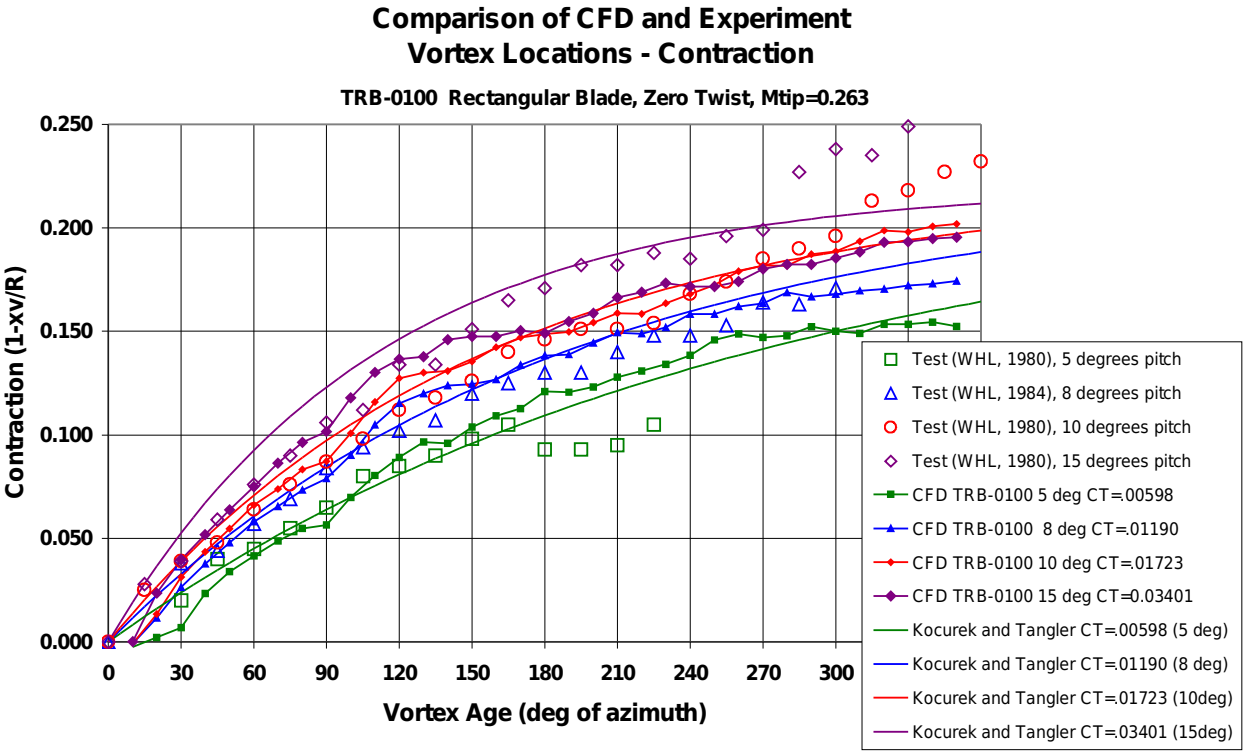

Figure 4. *Comparison between experiments and CFD predictions for the location of the tip vortex for the baseline blade. The solid lines represent predictions made with a Kocurek and Tangler wake model [10].*

Figure 5. *Planforms of the tail-rotor blade designs considered in this work. Variants of the datum blade with 8 and 16 degrees linear twist were also produced.*

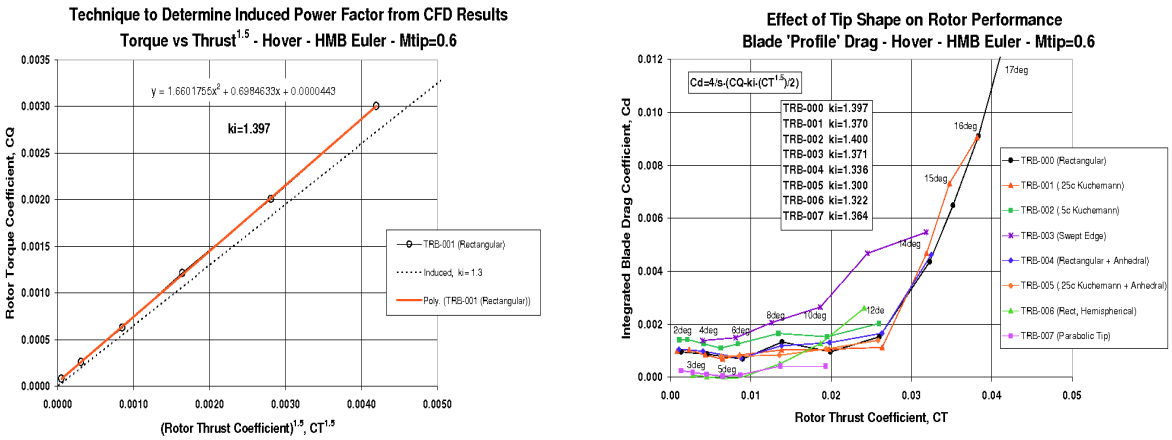

(a) (b)

Figure 6. *Technique to determine k_i, (a) example of fit to C_Q-$C_T^{1.5}$ for the datum blade, and (b) residual 'profile-power' due to Euler losses*

(a)

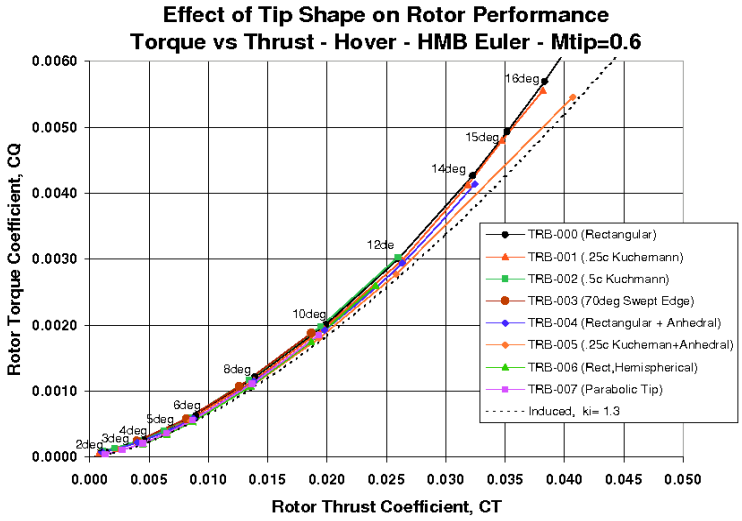

(b)

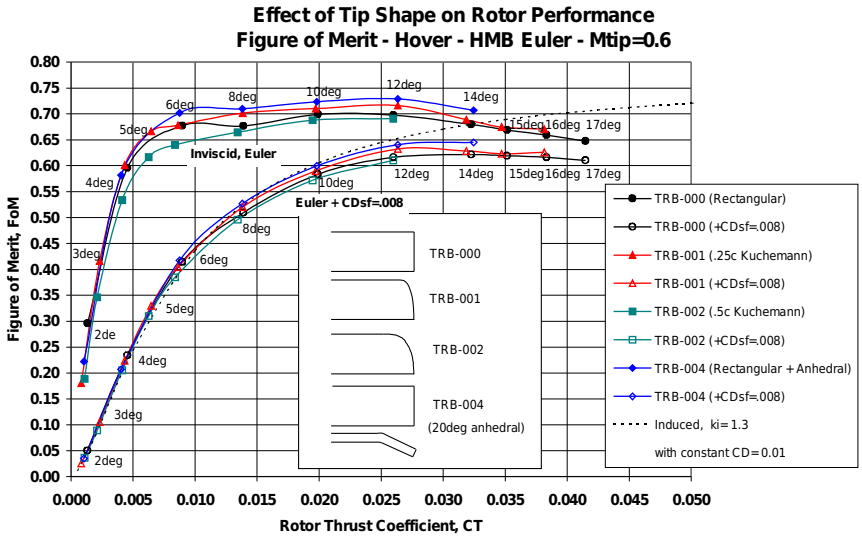

(c)

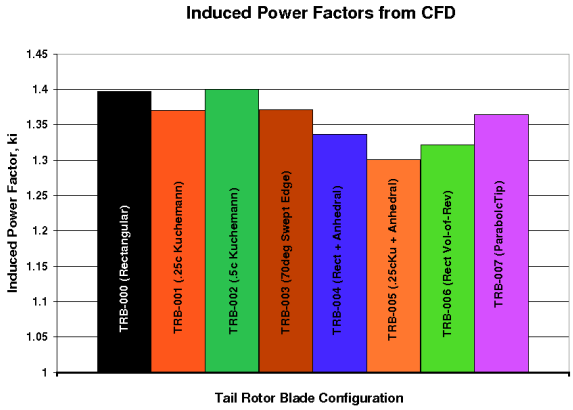

Figure 7. *Comparison of tail rotor designs in terms of (a) C_Q-C_T, (b) Figure of Merit (raw Euler results and with simple skin friction corrections, and (c) induced power factors.*

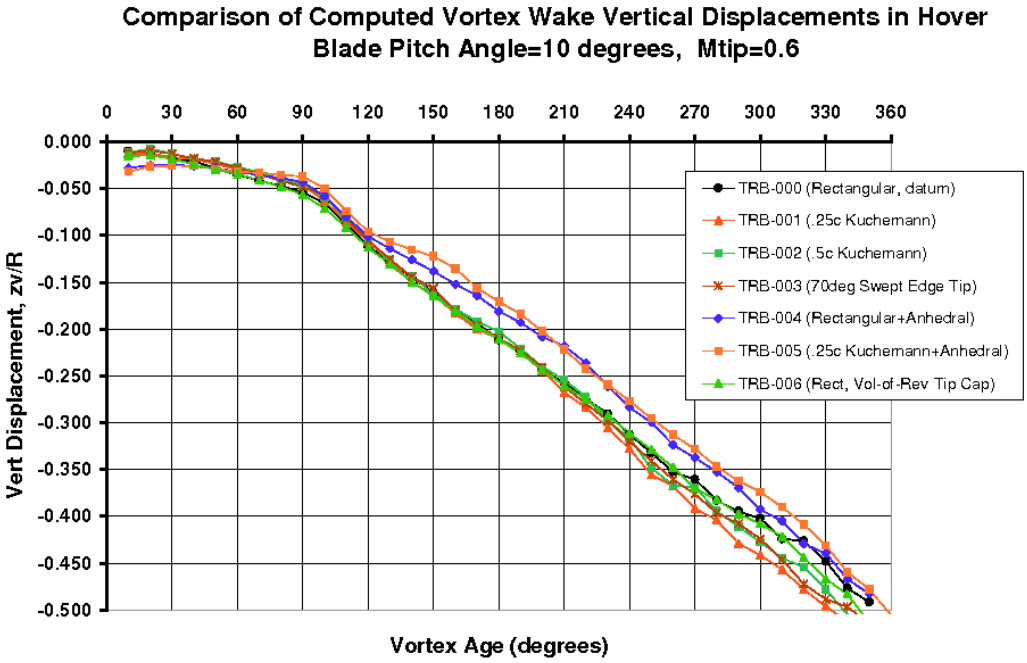

Figure 8. *Comparison of all tail rotor designs in terms of vertical vortex displacement.*

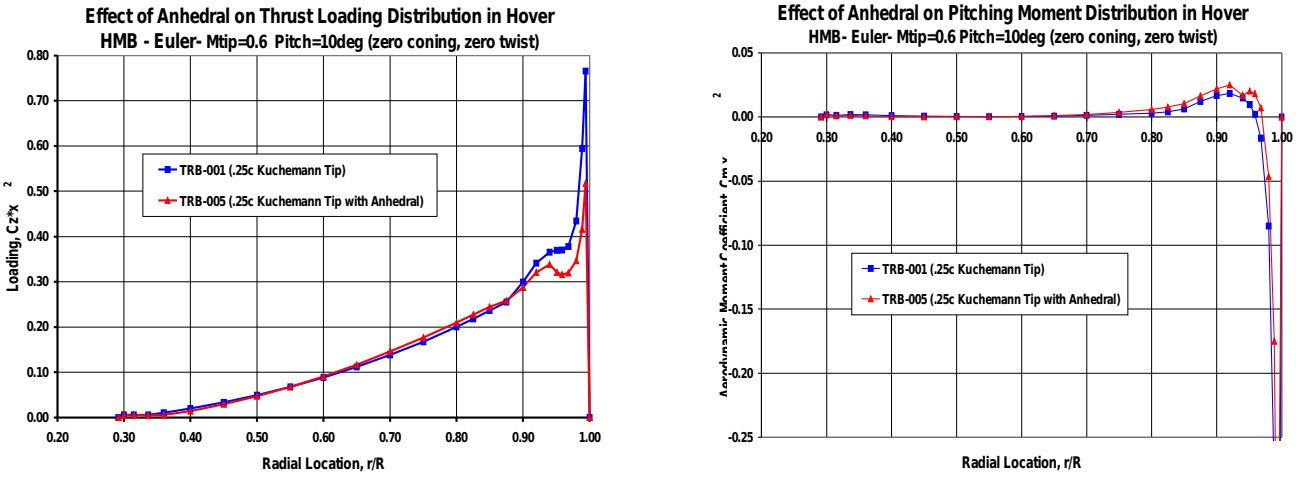

Figure 9. *Assessment of the effect of tip anhedral on (a) the span-wise loading, and (b) pitching moment distribution of a tail rotor.*

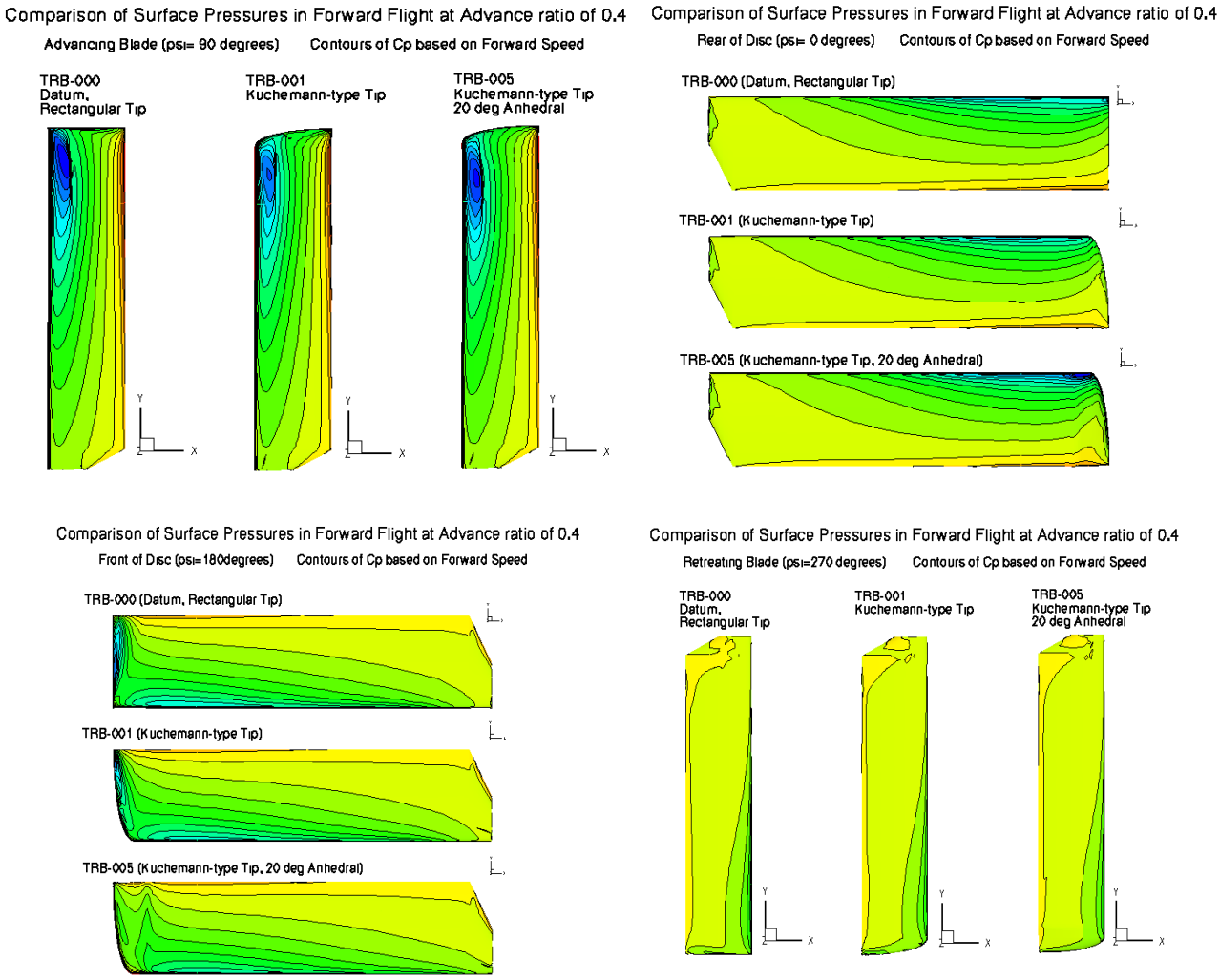

Figure 10 *Surface Pressure Contours at 0, 90, 180 and 270 degrees for the 3 selected tail rotor blades in forward flight at an advance ratio of 0.4 (M_{tip}=0.6, M_{adv}=0.84).*

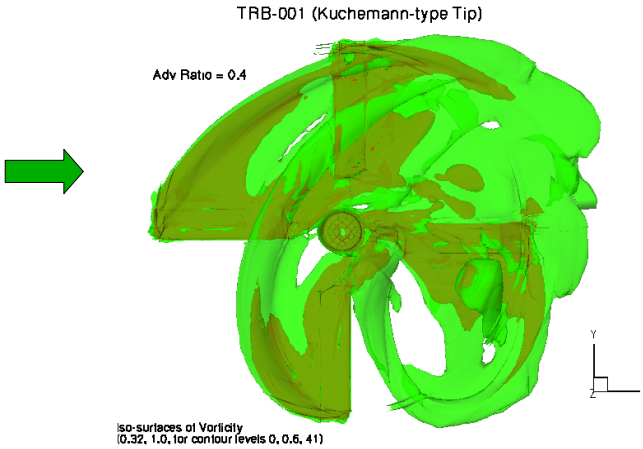

Figure 11. *Iso-surfaces of vorticity for TRB-001 (Kuchemann Tip) in forward flight showing vortex ahead of retreating blade.*

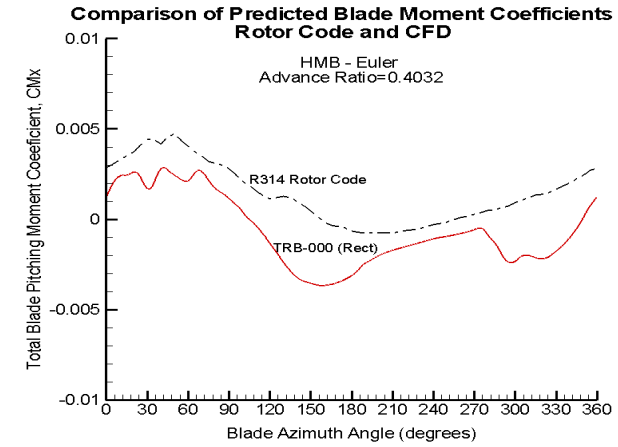

(a)

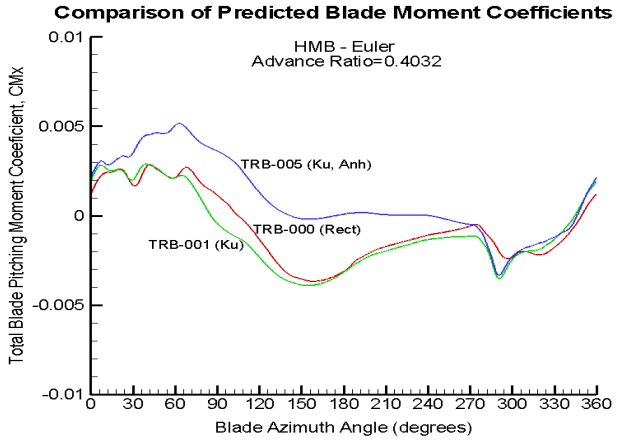

(b)

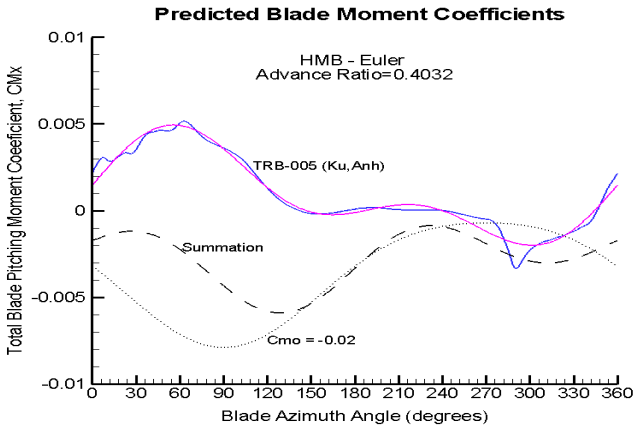

(c)

Figure 12. *Azimuthal Variation of Total Blade Aerodynamic Pitching Moments, (a) compared to lower order method , (b) effect of anhedral, (c) with cambered aerofoil.*

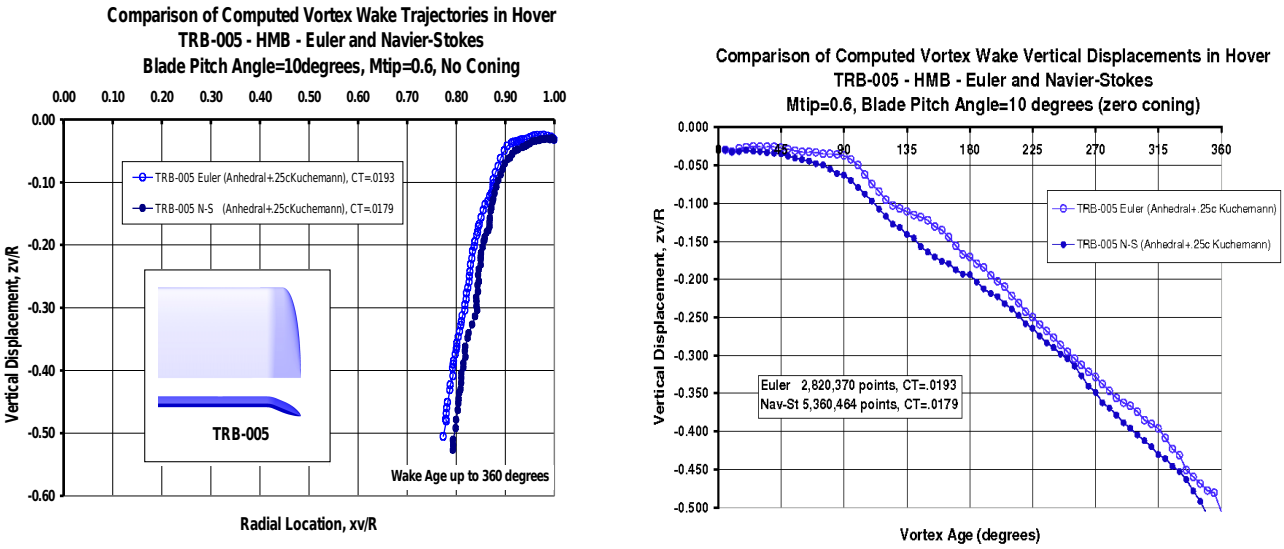

(a) *(b)*

Figure 13. *Vortex wake trajectories extracted from viscous CFD results for the anhedral blade, (a) reduced final contraction for N-S compared to Euler, (b) increased vertical displacement compared to Euler.*

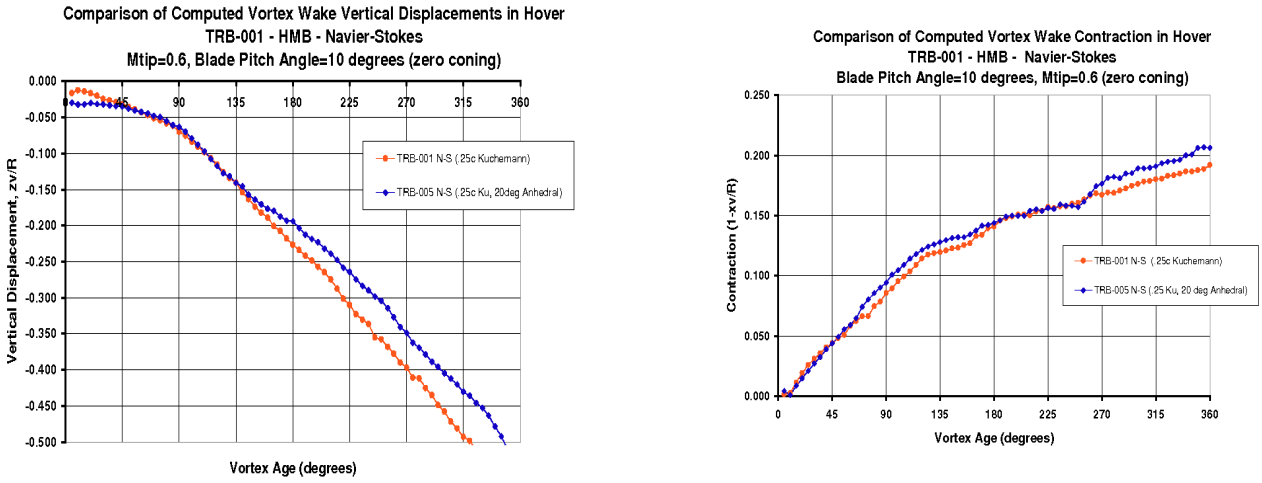

(a) *(b)*

Figure 14. *Comparison of vortex wake trajectories for tail rotor blades with and without anhedral, (a) vortex displacement for anhedral tip closer to blade, and (b) only small differences are seen in the wake contraction, with the anhedral blade producing slightly greater final contraction.*

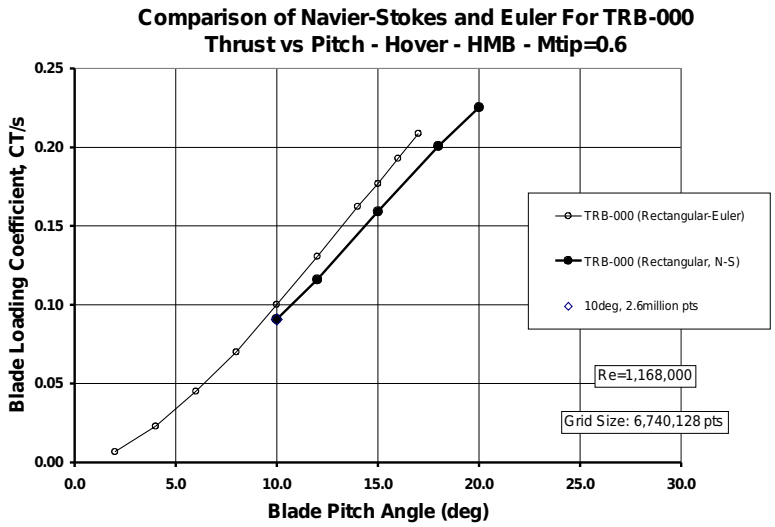

(a) Thrust-Pitch Characteristics

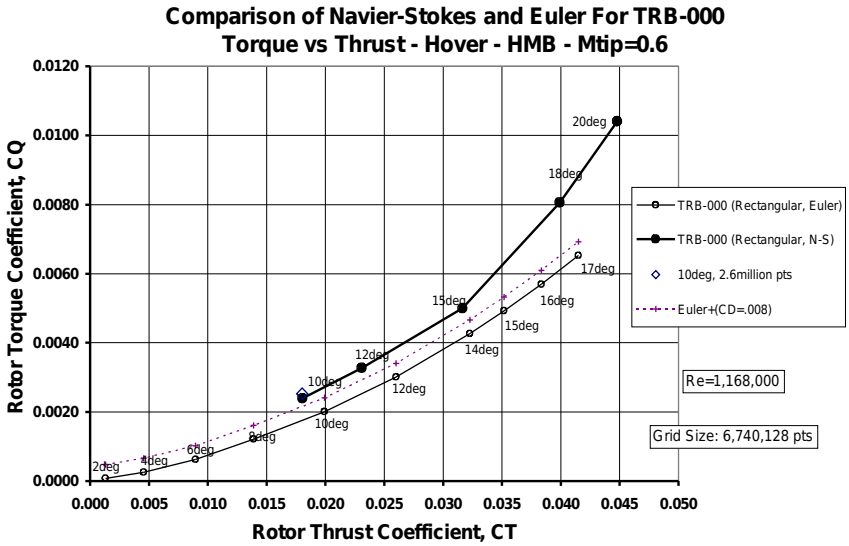

(b) Torque – Thrust Performance

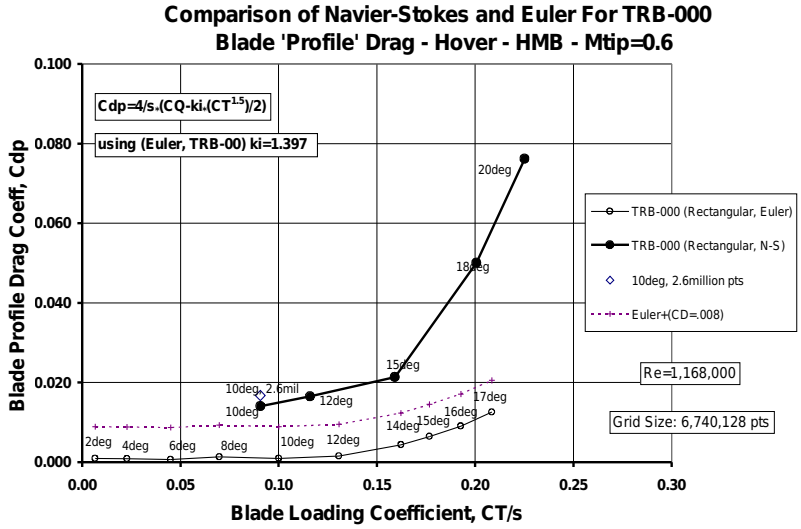

(c) Profile Power

Figure 15. *Navier-Stokes predictions for tail rotor performance at 10, 12, 15, 18 and 20 deg compared to Euler (a) CT/s-Pitch, (b) CT-CQ, (c) CD-CT/s.*

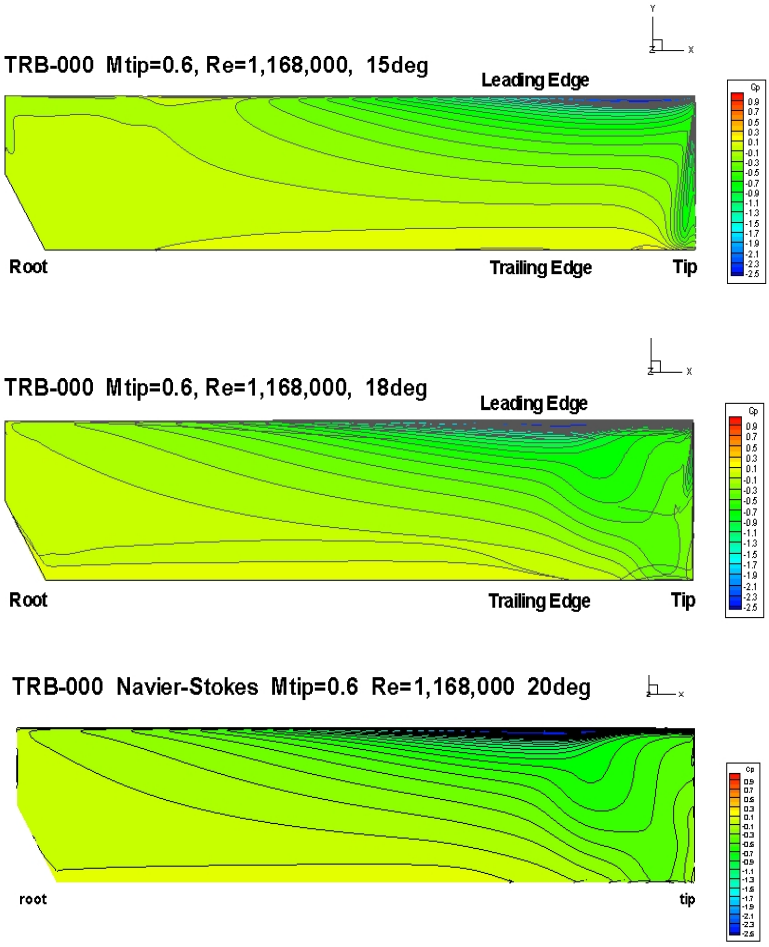

Figure 16. *Pressure Contours from Navier-Stokes CFD simulations indicate attached flow at up to 15 degrees, and flow separation near the tip at higher pitch.*

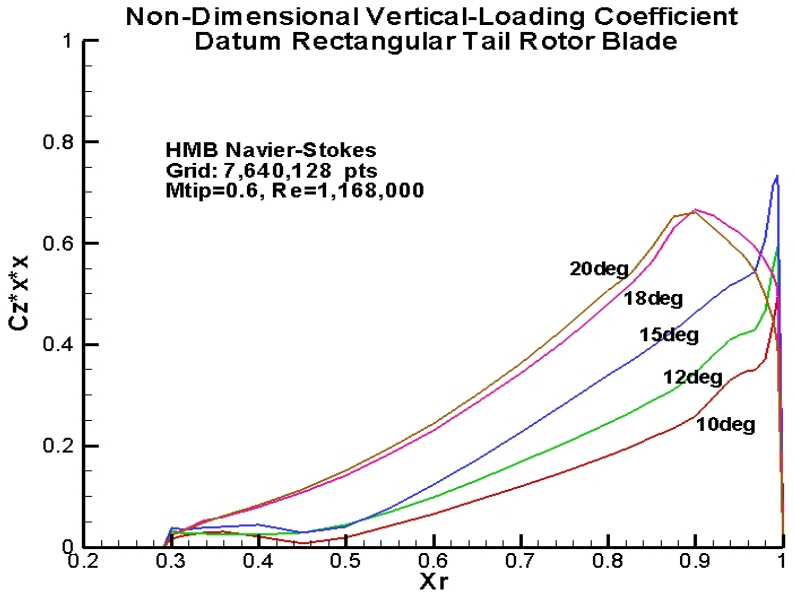

Figure 17. *Loading distribution in attached flow at 10, 12 and 15 deg, and effect of separation near the tip for 18 and 20 degrees pitch.*

Figure 18. *Experimental Set-up for Tail Rotor Fin-Blockage Tests (WHL 1980).*

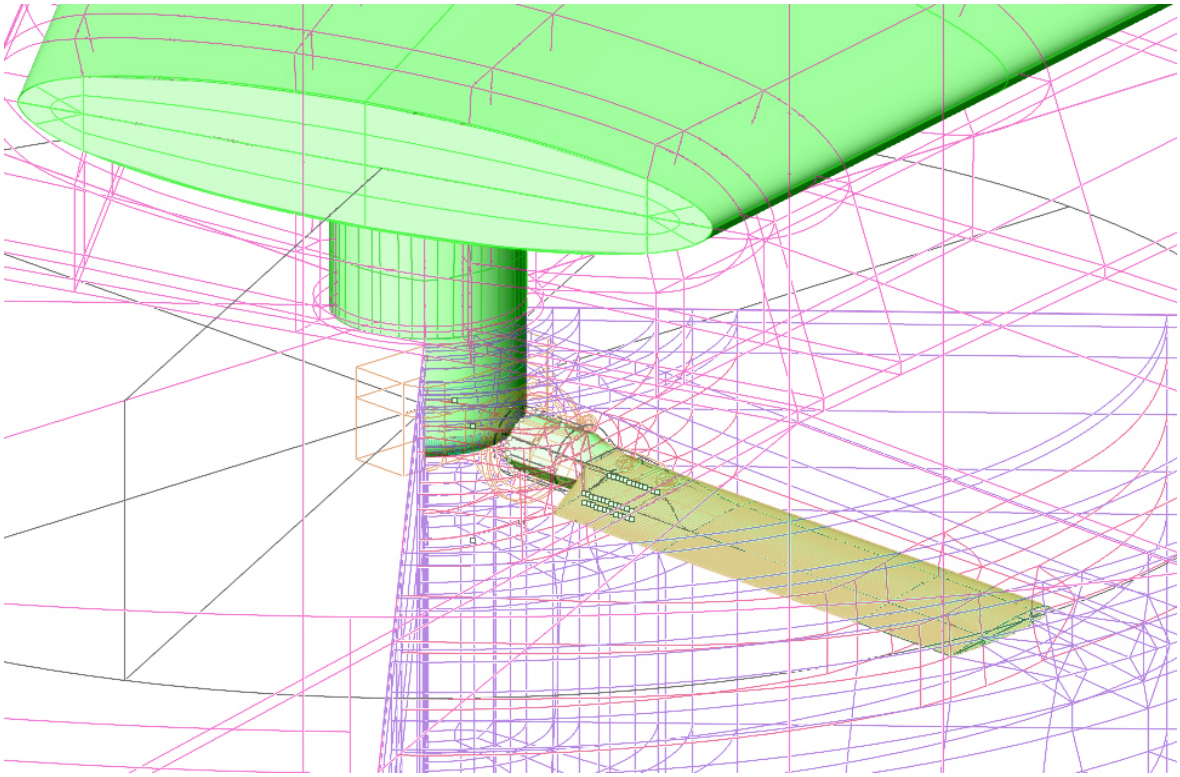

Figure 19. *Equivalent Geometry Set up for Tail Rotor Fin-Blockage Unsteady Navier-Stokes Simulations with Sliding Plane between Rotor and Fin.*